AIAA 2003–0265

Detached Eddy Simulation of the Flow over an Axisymmetric Cavity

Aroon K. Viswanathan, Kyle D. Squires
MAE Department, Arizona State University, Tempe, AZ

James R. Forsythe
United States Air Force Academy, Colorado Springs, CO

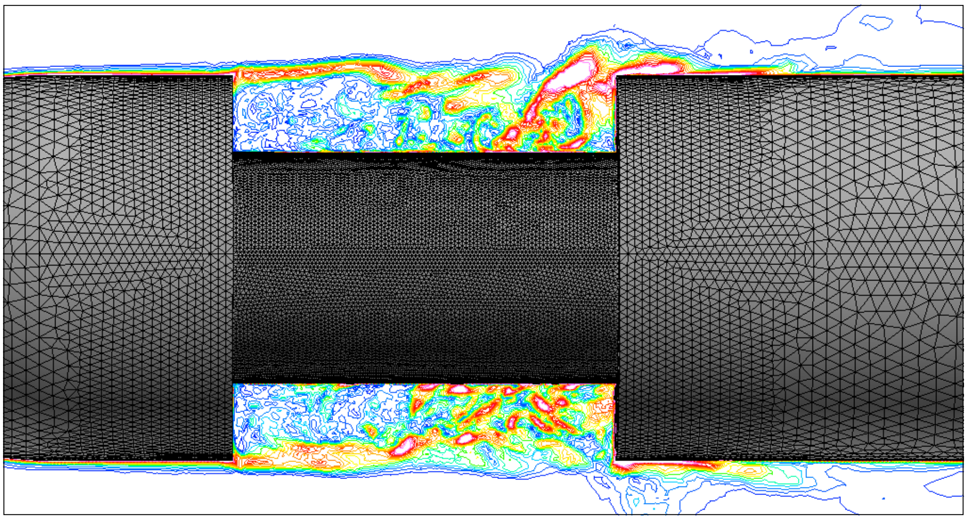

Aerospace Sciences Meeting 2003
6–9 January 2003 / Reno, Nevada

Detached Eddy Simulation of the Flow over an Axisymmetric Cavity

Aroon K. Viswanathan,* Kyle D. Squires†
MAE Department, Arizona State University, Tempe, AZ
James R. Forsythe‡
United States Air Force Academy, Colorado Springs, CO

Detached-Eddy Simulation (DES) is used to predict the flow over an axisymmetric cavity. The freestream Mach number is 0.4, the length-to-depth ratio of the cavity is equal to five. The main objectives are to characterize the instantaneous and mean properties of the solution, with a focus on the application of adaptive mesh refinement for improving the efficiency and fidelity of DES predictions. Computations were performed on unstructured meshes with cell sizes of 4×10^6 and 5.9×10^6 elements. The finer mesh was adaptively refined from the coarser grid such that cell densities were increased by about a factor of three in the cavity. The initially axisymmetric shear layer detaching from the front lip breaks down and the flow develops a range of scales within the cavity, the adaptively refined mesh leading to a deeper range of eddies. Flow visualizations and the mean pressure coefficient along the lower wall indicate that the oscillations in the cavity take place in shear layer mode. DES predictions of the Strouhal number corresponding to the fundamental and first harmonic are in reasonable agreement with Rossiter's formula.

Introduction

THE flow over cavities is relevant to an array of applications, e.g., that occurring near the bomb bays and/or landing gear housing of fighter aircraft. The flows are complex, being inherently unsteady in many regimes of practical interest and prone to acoustic resonance. Resonance leads to large fluctuations in pressure that may adversely affect the function of control systems and eventually lead to the catastrophic failure of structures. While prediction of resonant frequencies can be estimated in some regimes using analytical means [1], predicting the amplitude of pressure oscillations is not trivial. Additionally, the extrapolation of analytical approaches to more complex settings remains problematic.

As summarized by Shieh [2] and observed by several researchers (Ref. [1], [3], [4], and [5]), pressure oscillations consist of periodic and random components and the overall characteristics of the flow behavior depend on the geometry of the cavity, the incoming boundary layer thickness, and the Mach number M. Cavities can be classified as shallow or deep based on their length-to-depth ratio, L/D [1], the cavity considered in the present investigations is shallow, with $L/D = 5$. Also important is the mode of oscillation, in two-dimensional cavities, for example, increases in L/D lead to transitions from the shear layer mode to the wake mode, first noted in experiments by Gharib [6] and subsequently by Colonius [7] using Direct Numerical Simulation.

Cavity oscillations that occur in the shear layer mode are periodic. The dominant frequency is dependent on the flow Mach number and can be predicted using Rossiter's formula[1]. Power spectra yield a narrow band of frequencies in this case and for the shear layer mode the vortical structures in the cavity are smaller than the cavity depth. Consequently, the flow outside passes over the cavity reattaching at the rear lip. For cavity oscillations that occur in wake mode, large-scale vortex shedding results in a more random character to the flow that is independent of the Mach number. Frequency bands in the spectra are broader. The vortical structures are larger than the depth of the cavity and separation of the boundary layer downstream of the rear lip occurs due to the interactions of the shed structures with the wall.

Objectives

Computational approaches are an important element in understanding the underlying flowfield in cavities and offering a flexible tool for investigation of control strategies, among other aspects. This study constitutes the pre-cursor to a larger program that aims to combine experimental measurements with Computational Fluid Dynamics (CFD) to study resonance and its effect on cavities and to eventually develop control strategies that can be tested initially on simple configurations and eventually applied in practical applications.. In this work, the main goal is to apply CFD to predict the flow field and resulting pressure fluctuations within an axisymmetric cavity. The com-

*Research Assistant
†Professor, AIAA Member
‡AIAA Senior Member, present affiliation: Cobalt Solutions LLC

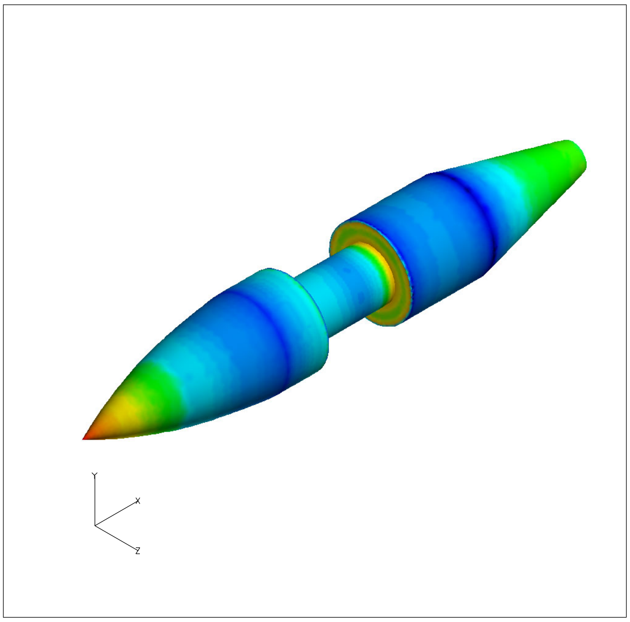

Fig. 1 Axisymmetric cavity with length $L = 6$ inches, depth $D = 1.2$ inches. Front lip located $2L$ downstream of the beginning of the circular ogive. Minimum diameter $= 1.5D$, Maximum diameter $= 2.5D$, $M_\infty = 0.4$.

putational technique applied is Detached-Eddy Simulation (DES), a hybrid RANS-LES technique that was originally designed for application to massively separated flows [8]. To date, DES has been applied to a number of complex flows, yielding predictions superior to that which can be obtained using Reynolds-averaged methods and usually outside the Reynolds number range for which Large Eddy Simulation (LES) is feasible [9] [10]. Shieh [2] applied DES to prediction of a two- and three-dimensional cavity, both with L/D equal to 4.4 and for a Mach number of 0.6. The two cases showed strikingly different behavior, with the two-dimensional cavity oscillating in wake mode and the three-dimensional cavity in shear layer mode.

In natural applications of the technique, DES reduces essentially to prediction of attached boundary layers using a Reynolds-averaged Navier-Stokes (RANS) approach and becomes a Large Eddy Simulation in regions away from the wall where there is sufficient grid density. In flows characterized by massive separation, development of eddy content in the detached regions occurs though a rapid adjustment and the modeling error associated with the lack of turbulent structure in the RANS boundary layers is negligible (e.g., see Squires *et al.* [9]). As DES is advanced beyond its design regime of massively separated flows, error sources due to effects such as the development of eddy content in the boundary layer may become more important. For the shallow cavity considered in this effort, application of the model assists in developing a framework for improving understanding of such issues.

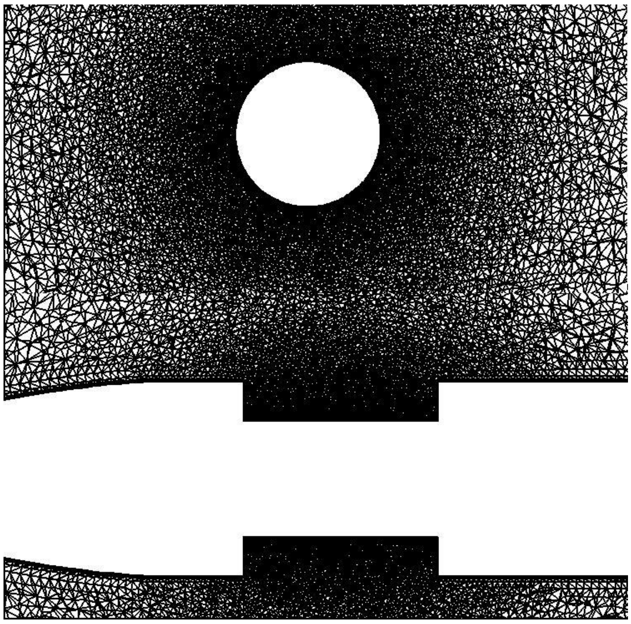

Fig. 2 Baseline grid. Mesh comprised of prisms in the boundary layer, tetrahedra away from the wall with 4×10^6 elements.

Simulation Model

The geometry is shown in Figure 1, a three-dimensional axisymmetric cavity which consists of a circular ogive section upstream. The ogive section is 12 inches in length and connects to a cylindrical section (six inches in diameter) that extends an additional three inches. The section consisting of the ogive and cylinder is sufficiently contoured that flow separation does not occur upstream of the cavity. The length L of the cavity is six inches, the depth D is equal to 1.2 inches, yielding $L/D = 5$. Downstream of the cavity is a smooth taper, which is effective for minimizing vibrations in this region. The tapered section also assists in preventing separation of the flow upstream of the cavity, ensuring that the fluctuations in the forces on the body are the result of interactions that occur only within the cavity. The Mach number and Reynolds number per unit length are 0.4 and 1.8×10^5, respectively.

Grid design and adaptive mesh refinement

Unstructured grids were used to resolve the flowfield over and within the cavity. The grids were created using Gridtool [11] and VGRIDns [12]. Gridtool is an interface used to develop the surface point distributions and background sources, VGRIDns is used to create the volume grid within the domain. The initial (baseline) grid was generated with a higher density of points within the cavity (c.f., Figure 2). The average spacing from solid surfaces to the first cell center nearest the wall was within one viscous unit, grids were geometrically stretched at a rate 1.2 within the boundary layer

An important grid technology that is well suited

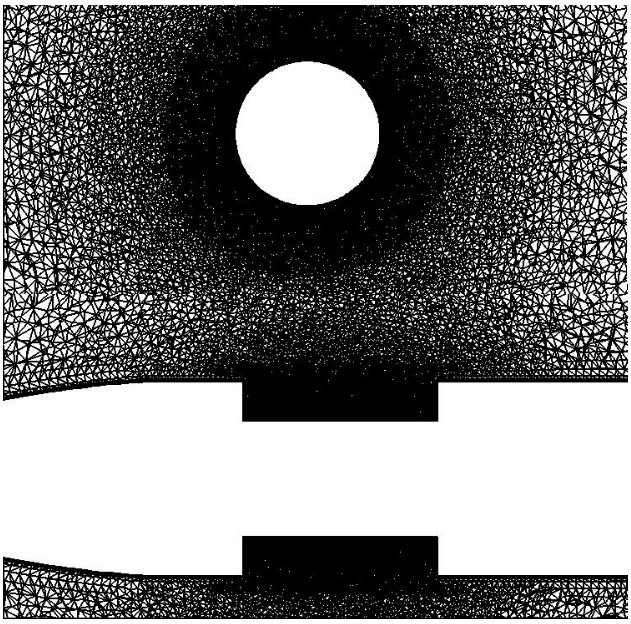

Fig. 3 Adapted grid. Adapted grid comprised of 5.9×10^6 elements.

for DES is adaptive mesh refinement. Pirzadeh [13] has developed a method based on a tetrahedral unstructured grid technology and applied the method to configurations with vortex-dominated flowfields. Mitchell *et al.* [14] have applied the approach to DES predictions of the flow over a delta wing, yielding comparable accuracy in predicting effects such as vortex breakdown using solution-adapted meshes that contained far fewer points then denser grids in which refinement had been applied globally.

Mesh adaption is applied to the current configuration using the method developed by Pirzadeh [13]. In this approach, adaption can be applied in a user-specified region or may be based on a flow variable determined from a pre-existing calculation. Variables such as vorticity, entropy, and pressure gradient can be employed as thresholds for identifying regions for adaption. The region is 'carved out' of the existing mesh and a denser grid is created, the increase in the density controlled by the factor *ifact* in VGRIDns. For the work presented here, a cylindrical region around the cavity was isolated for adaption. An example of adaptively refining the grid is shown in Figure 3. For the results shown below, the baseline mesh was comprised of 4×10^6 elements with adaption to 5.9×10^6 elements. While the overall increase in the number of cells is a factor of nearly 1.5, the increase in the cell density within the cavity is closer to three. Both grids consist of prism layers in the boundary layers near solid surfaces and nearly isotropic tetrahedra elsewhere.

Detached Eddy Simulation

The three-dimensional, time dependent flow in the cavity was predicted using Detached Eddy Simulation. The DES formulation is based on a modification to the Spalart-Allmaras RANS model [15] such that the model reduces to its RANS formulation near solid surfaces and to a subgrid model away from the wall [8]. The transport equation for the working variable $\tilde{\nu}$ used to form the eddy viscosity takes the form,

$$\begin{aligned}\frac{D\widetilde{\nu}}{Dt} &= c_{b1}\widetilde{S}\,\widetilde{\nu} - \left[c_{w1}f_w - \frac{c_{b1}}{\kappa^2}f_{t2}\right]\left[\frac{\widetilde{\nu}}{d}\right]^2 \\ &+ \frac{1}{\sigma}\left[\nabla\cdot((\nu+\widetilde{\nu})\nabla\widetilde{\nu}) + c_{b2}\,(\nabla\widetilde{\nu})^2\right], \quad (1)\end{aligned}$$

where $\widetilde{\nu}$ is the working variable. The eddy viscosity ν_t is obtained from,

$$\nu_t = \widetilde{\nu}\, f_{v1} \qquad f_{v1} = \frac{\chi^3}{\chi^3 + c_{v1}^3} \qquad \chi \equiv \frac{\widetilde{\nu}}{\nu} \quad (2)$$

where ν is the molecular viscosity. The production term is expressed as,

$$\widetilde{S} \equiv S + \frac{\widetilde{\nu}}{\kappa^2 d^2} f_{v2}\,, \qquad f_{v2} = \left(1 + \frac{\chi}{c_{v2}}\right)^{-3}, \quad (3)$$

where S is the magnitude of the vorticity. The function f_w is given by,

$$\begin{aligned} f_w &= g\left[\frac{1+c_{w3}^6}{g^6 + c_{w3}^6}\right]^{1/6} \\ g &= r + c_{w2}\,(r^6 - r) \\ r &\equiv \frac{\widetilde{\nu}}{\widetilde{S}\kappa^2 d^2}\,. \quad (4)\end{aligned}$$

The wall boundary condition is $\widetilde{\nu} = 0$. The constants are $c_{b1} = 0.1355$, $\sigma = 2/3$, $c_{b2} = 0.622$, $\kappa = 0.41$, $c_{w1} = c_{b1}/\kappa^2 + (1 + c_{b2})/\sigma$, $c_{w2} = 0.3$, $c_{w3} = 2$, $c_{v1} = 7.1$, $c_{v2} = 5$, $c_{t1} = 1$, $c_{t2} = 2$, $c_{t3} = 1.1$, and $c_{t4} = 2$.

In DES, the distance to the nearest wall d is replaced by $\tilde{d}$,

$$\tilde{d} \equiv min(d, C_{DES}\Delta)\,, \quad (5)$$

where Δ is the maximum distance between the centroid of the cell to the centroids of the neighbouring cells. In "natural" applications of DES, the wall-parallel grid spacings (e.g., streamwise and spanwise) are on the order of the boundary layer thickness and the S-A RANS model is retained throughout the boundary layer, i.e., $\widetilde{d} = d$. Consequently, prediction of boundary layer separation is determined in the "RANS mode" of DES. Away from solid boundaries, the closure is a one-equation model for the sub-grid scale eddy viscosity. When the production and destruction terms of the model are balanced, the length scale $\widetilde{d} = C_{DES}\Delta$ in the LES region yields a Smagorinsky-like eddy viscosity $\widetilde{\nu} \propto S\Delta^2$. Analogous to classical LES, the role of Δ is to allow the energy cascade down to the grid size. The additional model constant $C_{DES} = 0.65$ was set in homogeneous turbulence [16].

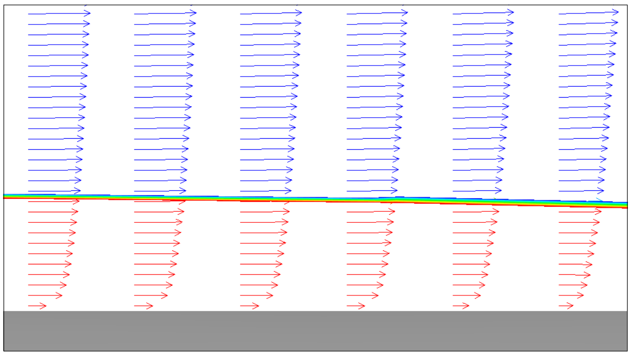

Fig. 4 Velocity vectors on the upstream section prior to the front lip of the cavity. Line shows the border of the RANS and LES regions.

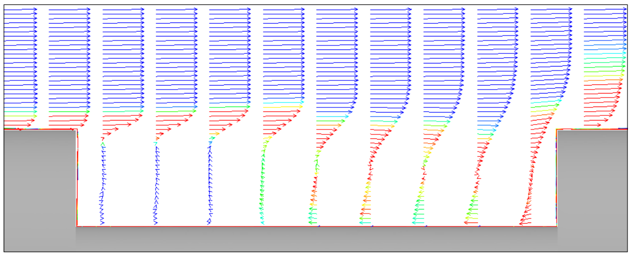

Fig. 5 Velocity vectors inside and above the cavity shown at intervals $0.1D$. Vectors colored by turbulent eddy viscosity.

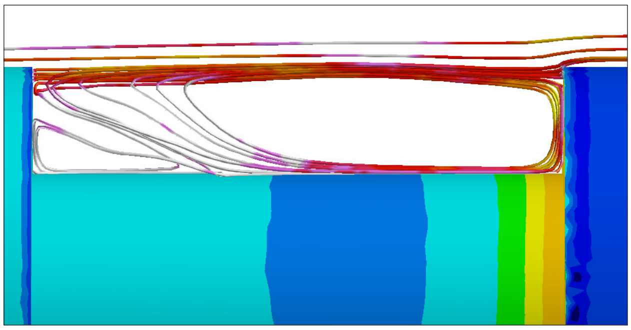

Fig. 6 Mean flow streamlines in the cavity region for the baseline grid. Geometry colored with pressure. Streamlines colored by mean vorticity magnitude

Flow solver

The compressible Navier-Stokes equations are solved on unstructured grids using Cobalt [17], a commercial version of Cobalt$_{60}$, the Navier-Stokes solver developed at the Air Force Research Laboratory. The numerical method is a cell-centered finite volume approach applicable to arbitrary cell topologies (e.g, hexahedrals, prisms, tetrahedrons). The spatial operator uses the exact Riemann Solver of Gottlieb and Groth[18], least squares gradient calculations using QR factorization to provide second order accuracy in space, and TVD flux limiters to limit extremes at cell faces. A point implicit method using analytic first-order inviscid and viscous Jacobians is used for advancement of the discretized system. For time-accurate computations, a Newton sub-iteration scheme is employed, the method is second order accurate in time. The domain decomposition library ParMETIS [19] is used for parallel implementation and provides optimal load balancing with a minimal surface interface between zones. Communication between processors is achieved using Message Passing Interface.

Results

Calculations were performed at a freestream Mach number of 0.4 and at an ambient pressure 11.4 psi. The corresponding Reynolds number per unit length was 1.8×10^5. The timestep, made dimensionless using the freestream speed and cavity length L was 0.022. Following the development of an initial transient in the solutions, the flow achieved a statistically stationary condition, monitored by the time histories of the forces acting on the cavity. Once the flow achieved equilibrium, cavity pressures at several points along the sides and lower wall were sampled at a rate of 2000 Hz. DES predictions for both grids showed that the flow remained attached to the body with the boundary layer thickness growing to approximately $0.25D$ just upstream of the front lip.

Shown in Figure 4 are mean velocity vectors in a section upstream of the cavity. The vectors are shown from the solution obtained on the adapted grid and drawn in the figure is the interface between the RANS and LES regions. The wall-normal location of the interface is about $0.02D$, smaller than the boundary layer thickness which is closer to $0.2D$. Thus, much of the boundary layer lies outside of the RANS region, above the RANS region this part of the profile will be treated with a turbulence closure in which the destruction term has been reduced via the lengthscale re-definition (5).

Mean-flow velocity vectors within and above the cavity are shown in Figure 5. The figure shows that the mean velocity in the cavity is characterized by a large recirculation that extends upstream more than half the cavity length. The peak reverse-flow velocity near the wall is about 1/3 of the peak forward-flow velocity. The mean streamlines in Figure 6, shown from predictions on the baseline grid, are consistent with the vectors in Figure 5, also showing a smaller recirculating region in the lower front corner of the cavity. The flow tends to remain attached downstream of the cavity and the size of the larger vortical structures as observed from the streamlines remains smaller than the cavity depth. Both figures are characteristic of the shear layer mode at which the present cavity oscillates, as discussed by Shieh [2], among others.

Flow structure resolved by the two grids, i.e., the baseline mesh of 4×10^6 elements and adapted grid of 5.9×10^6 elements are shown in Figure 7, Figure 8, and Figure 9. The figures show contours of the instantaneous vorticity in planes normal to the

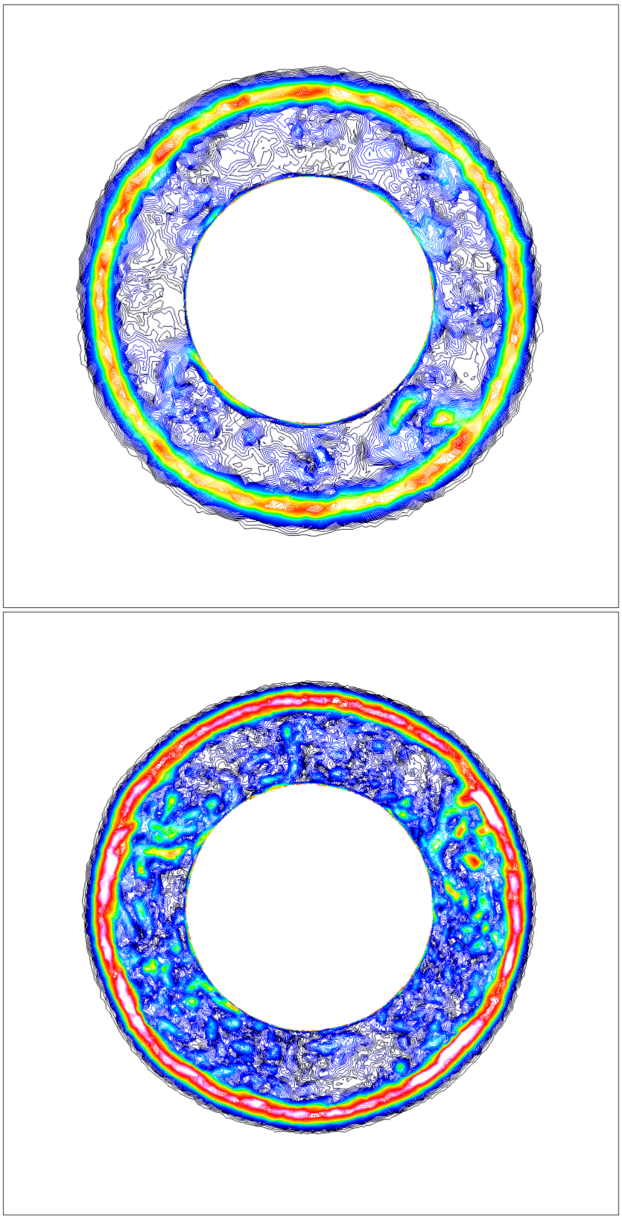

Fig. 7 Instantaneous vorticity in the DES predictions on the baseline (upper frame) and adapted (lower frame) grids, $x/L = 0.167$.

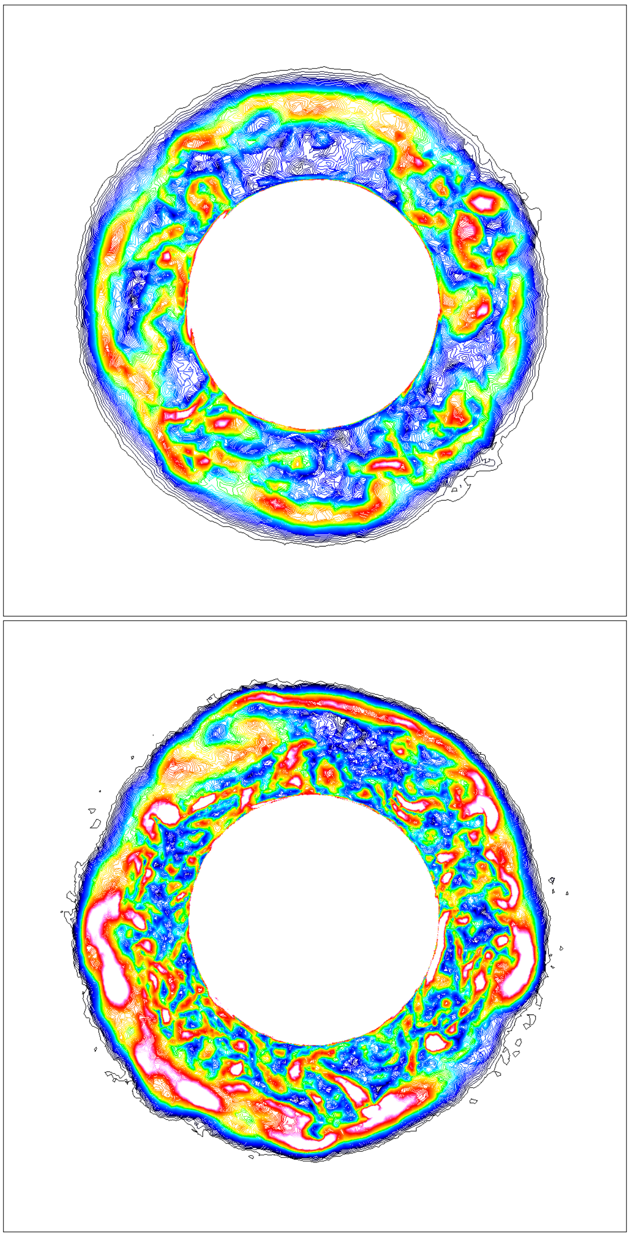

Fig. 8 Instantaneous vorticity in the DES predictions on the baseline (upper frame) and adapted (lower frame) grids, $x/L = 0.5$.

freestream velocity at axial locations near the front ($x/L = 0.167$) in Figure 7, middle ($x/L = 0.50$) in Figure 8 and rear ($x/L = 0.833$) in Figure 9. At $x/L = 0.167$, the detaching shear layer is relatively intact as shown by the axisymmetric contours marking the peak vorticity in Figure 7. While the two grids yield comparable features, peak vorticity levels in the adapted grid are approximately 25% higher than in the baseline mesh, a consequence of the adaption over this region. In the mid-plane at $x/L = 0.50$ shown in Figure 8 the adapted grid exhibits a deeper range of scales than is achieved on the baseline mesh. As also true at $x/L = 0.167$, peak vorticity levels are about 25% higher on the adapted mesh. Compared to Figure 7, the flow is more chaotic and without a clear axisymmetric structure as apparent at $x/L = 0.167$. At $x/L = 0.833$, the difference in the range of scales resolved on the baseline and adapted grids shown in Figure 9 is the most pronounced with many more regions (red in the figure) of intense vorticity captured on the adapted mesh. The solutions are the most chaotic at this axial station compared to the two streamwise locations upstream.

The instantaneous vorticity contours along the cavity, shown in Figure 10, show the development of an array of vortical structures with downstream evolution and the wider scale range resolved on the adapted grid. Vorticity contours from the prediction obtained in the baseline grid appear to indicate a lateral oscillation of

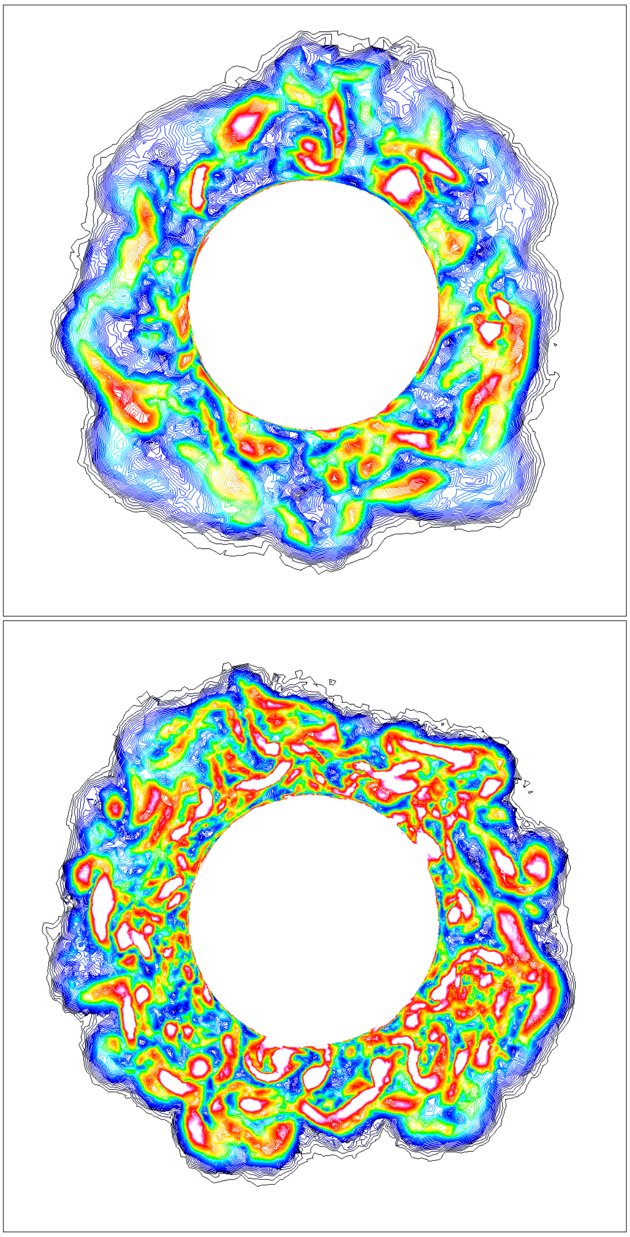

Fig. 9 Instantaneous vorticity in the DES predictions on the baseline (upper frame) and adapted (lower frame) grids, $x/L = 0.833$.

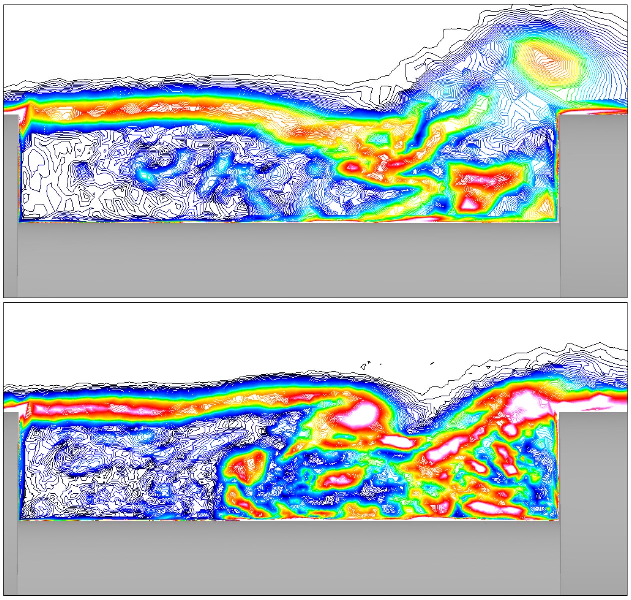

Fig. 10 Instantaneous vorticity in the DES predictions on the baseline (upper frame) and adapted (lower frame) grids.

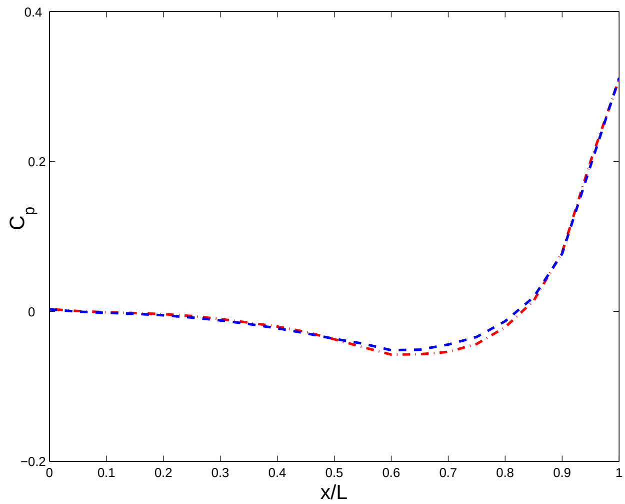

Fig. 11 Pressure coefficient along the cavity wall. Red line: baseline grid; Blue line: adapted grid.

the structures, with shedding just above the rear lip of the cavity. There exists near the rear of the cavity, a region of interaction between the external flow and that within the cavity, resulting in an exchange of mass and momentum between the two layers, which is a characteristic of three-dimensional cavity flows. In addition, computations showed that the boundary layer on the downstream section remains mostly attached unlike for cavities in wake mode where the ejected structures can interact with the downstream section and cause boundary layer separation.

The mean pressure coefficient on the lower cavity wall is shown in Figure 11. Over the initial half of the lower wall, the pressure is uniform, becoming slightly negative over the region $0.6 < x/L < 0.8$, the reduction in pressure arising due to the recirculating motion that characterizes the mean velocity and, in particular, the high reverse-flow velocities in this region (c.f., Figure 5). Past $x/L = 0.8$, the flow stagnates as it encounters the rear cavity wall, the figure showing an increase in C_p to about 0.3.

The Strouhal numbers of the oscillation modes were determined from power spectral densities of the pressure histories. The predicted Strouhal numbers for the first two modes of oscillation are shown in Figure 12. Also shown in the figure are predictions obtained using Rossiter's formula,

$$St = \frac{f_m L}{U} = \frac{m - \alpha}{M + 1/\kappa}, \qquad (6)$$

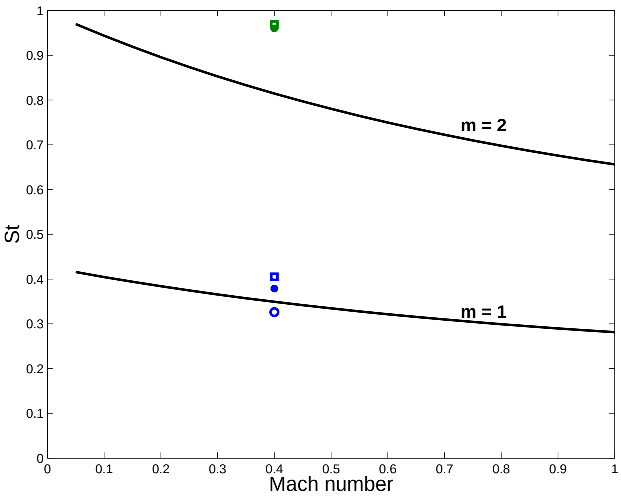

Fig. 12 Predicted Strouhal numbers of the dominant frequencies. ——— Eqn. (6)

.

where m is the mode, f the dominant frequency of oscillation, U the freestream speed, M the freestream Mach number[1]. The factor $\alpha = 0.25$ is a constant related to the phase speed of the shear layer disturbance and k is the ratio of the vortex convection velocity across the cavity to the freestream speed. Power spectral densities of the pressure traces along the cavity wall at $x/L = 0.1$, 0.5, and 0.9 were processed, the Strouhal numbers corresponding to the dominant modes at these locations are shown in Figure 12. As shown on the figure, the Strouhal numbers for the first and second modes of oscillation are in the range 0.37 and 0.96, respectively. Agreement with the predicted first mode from (6) of 0.38 is very good, the simulations are above the second mode obtained from (6) of 0.88.

Summary

The flow over an axisymmetric cavity was predicted using Detached-Eddy Simulation, the main aim was to characterize the solution both in terms of its mean properties and the structural features resolved within the cavity. Mean streamlines and the mean pressure along the cavity wall are consistent with a shear layer mode of oscillation. A large recirculating structure that extends from the rear wall to roughly half the cavity length characterizes the mean flow, peak backflow velocities are comparable to the peak forward flow velocities.

One focus of the study was the application of adaptive mesh refinement, used to increase cell densities in the focus region comprising the cavity. On the finer mesh, the total number of cells increased by nearly a factor of 1.5. Because of adaptive mesh refinement, cell densities increased by nearly a factor of three within the cavity. Flow visualizations showed a tangibly deeper range of scales captured on the finer mesh, peak vorticity levels increased by about 25% from the baseline to the refined grid. Predictions of the Strouhal numbers of the first two modes of oscillation were in reasonable agreement with estimates obtained using Rossiter's formula.

In general, the meshes employed in these investigations are relatively fine, one issue is that the interface between the RANS and LES regions was within the boundary layer on the upstream section, prior to the cavity. In the LES region, the eddy viscosity is reduced and if the interface is sufficiently close to the wall, errors in quantities such as the skin friction and boundary layer thickness will become more prominent due to under-predictions of the turbulent stresses. More detailed studies are necessary to better understand these issues, as well as the cavity characteristics with changes in parameters such as the Mach number.

References

[1] Rossiter, J.E, "Wind Tunnel Experiments on the flow over Rectangular Cavities at subsonic and transonic speeds", Aeronautical Research Council, Reports and Memoranda, R&M No. 3438, 1966

[2] Shieh, C.M. and Morris, P.J., "Comparison of two dimensional and three dimensional turbulent cavity flows", *AIAA Paper 2001-0511*, 2001.

[3] Heller, H.H., Holmes, D.G., Covert, E.E., "Flow induced pressure oscillations in shallow cavities", *Journal of Sound and Vibration*, **18**(4), pp. 545-553, 1971.

[4] Khan, M.U., Hirahara, H., Kawahashi, M., "Experimental and numerical investigation on generation of sound resonance in a transonic cavity flow", Sixth Triennial International Symposium on Fluid control, measurements and visualization, FLUCOME, 2000, Aug. 13-17, 2000.

[5] Hamed, A., Basu, D., Mohamed, A., Das, K., "Direct Numerical Simulations of high speed flow over cavity", Third AFSOR International Conference on DNS/LES, August 5-9,2001.

[6] Gharib, M. and Roshko, A., "The efect of flow oscillations on cavity drag", *J. Fluid Mechanics*, **177**, pp. 501-530, 1987.

[7] Colonius, T., Basu, A.J. and Rowley, C.W. "Numerical Investigation of the flow past a Cavity", *AIAA Paper 99-1912*, 1999.

[8] Spalart, P.R., Jou, W.H., Streles, M. and Allmaras, S.R., " Comments on feasibility of LES for wings and on a hybrid RANS/LES approach", Proceedings of the First AFSOR International Conference on DNS/LES, Greyden Press, Columbus, OH, Ruston, LA, August 4-8 1997

[9] K.D. Squires, J.R. Forsythe, S.A. Morton, W.Z. Strang, K.E. Wurtzler, R.F. Tomaro, M.J. Grismer and P.R. Spalart, "Progress on Detached-Eddy Simulation of massively separated flows", *AIAA Paper 2002-1021*, 2002.

[10] Forsythe, J.R., Squires, K.D., Wurtzler, K.E., Spalart, P.R., "Detached-Eddy Simulation of Fighter Aircraft at High Alpha," *AIAA 2002-0591*, 2002.

[11] Jamshid, S.-A., "GridTool: A Structured Modeling and Grid Generation Tool", Proceedings of the Workshop on Surface Modelling. Grid Generation, and Related Issues in CFD Solutions, NASA CP-3291, 1995.

[12] Pirzadeh, S., "Three-dimensional Unstructured Viscous Grids by the Advancing Layers Method", *AIAA J.*, **34**, pp. 43-49, 1996.

[13] Pirzadeh, S., "Vortical Flow Prediction Using an Adaptive Unstructured Grid Method", Research & Technology Organization Applied Technology Panel Meeting, Norway, 7-11 May 2001.

[14] Mitchell, A.M., Morton, S.A. and Forsythe, J.R., "Analysis of Delta Wing Vortical Substructures using Detached-Eddy Simulation", *AIAA Paper 2002-2968*, 2002.

[15] Spalart, P.R., and Allmaras, S.R., "A One-Equation Turbulence model for Aerodynamic Flows", *La Recherche Aerospatiale*, **1**, pp. 5-21, 1994.

[16] Shur, M., Spalart, P.R., Strelets, M., and Travin, A, 1999, "Detached-Eddy Simulation of an Airfoil at High Angle of Attack", 4th Int. Symp. Eng. Turb. Modelling and Measurements, Corsica, May 24-26, 1999.

[17] Strang, W.Z., Tomaro, R.F. and Grismer, M.J., "The Defining Methods of Cobalt$_{60}$: a Parallel, Implicit, Unstructured Euler/Navier-Stokes Flow Solver," *AIAA 99-0786,* 1999.

[18] Gottlieb, J.J. and Groth, C.P.T, "Assessment of Riemann solvers for unsteady one-dimensional inviscid flows of perfect gases", *J. Comp. Physics*, **78**, pp. 437-458, 1988.

[19] Karypis, G., Schloegel, K. and Kumar, V, *ParMETIS: Parallel Graph Partitioning and Sparse Matrix Ordering Library Version 1.0*, University of Minnesota, Department of Computer Science, Minneapolis, MN 55455, July 1997.